Nuclear Science and Techniques (2025) 36:129
https://doi.org/10.1007/s41365-025-01726-z

Study of the nuclear mass model by sequential least squares programming

Hang Yang[1] · Cun-Yu Chen[1] · Xiao-Yu Xu[1] · Han-Kui Wang[1] · You-Bao Wang[2]

Received: 22 October 2024 / Revised: 3 January 2025 / Accepted: 26 January 2025 / Published online: 26 May 2025

Abstract

Nuclear mass is an important property in both nuclear and astrophysics. In this study, we explore an improved mass model that incorporates a higher-order term of symmetry energy using algorithms. The sequential least squares programming (SLSQP) algorithm augments the precision of this multinomial mass model by reducing the error from 1.863 MeV to 1.631 MeV. These algorithms were further examined using 200 sample mass formulae derived from the δE term of the E_{isospin} mass model. The SLSQP method exhibited superior performance compared to the other algorithms in terms of errors and convergence speed. This algorithm is advantageous for handling large-scale multiparameter optimization tasks in nuclear physics.

Keywords Nuclear mass model · Binding energy · Magic nuclei · Sequential least squares algorithm

1 Introduction

An atomic nucleus, which contains valuable information regarding atomic structure, is a fundamental physical property [1]. Changes in atomic mass directly affect the nuclear stability and energy release during nuclear reactions [2]. The mass of a neutron-rich nucleus plays a crucial role in fast neutron capture (the r-process) during stellar nucleosynthesis. Thus, studying mass is essential to comprehensively understand the formation and evolution of elements in the universe [3–5]. Recently, the development of radioactive ion beam facilities has led to experimental measurements of more than 3000 ground state atomic masses [6, 7], with studies continuously expanding to both sides of the β stability line. In astrophysics, large amounts of data concerning the masses of neutron-rich or neutron-poor nuclei in regions far from the stability line are required. This is difficult to measure directly using the current technology. Therefore, several mass models have been proposed.

In 1935, Bethe and Weizsacker proposed the semiempirical BW mass formula [8–10] that predicts mass with an accuracy of approximately 3 MeV. In Ref. [11], nuclear binding energy is divided into two parts: a large and smooth component and a small and fluctuating component. The classical droplet model only accounts for a smooth trend and fails to consider the rapid fluctuation of the binding energy around the shell gap with a number of protons and neutrons. This suggests that important physical effects are absent in the classical mass model [12, 13]. To solve this problem, physicists have developed macroscopic–microscopic mass models. These models introduce shell correction terms such as the finite force range droplet model (FRDM) [14], Koura–Tachibana–Uno–Yamada (KTUY) [15] and Lublin–Strasbourg drop (LSD) [16], and micromass models such as the Hartree–Fock–Bogoliubov (HFB) approach [17, 18] and relativistic mean-field (RMF) theory [19]. The cited research is primarily based on the density functional theory (DFT) [20]. Although DFT is more complex, it exhibits superior extrapolation capabilities.

Kirson et al. added six physical terms as constraints to the mass model [21–27]. The obtained BW2 mass model was improved to some extent by addressing the problems of

This work was supported by the National Natural Science Foundation of China (Nos.U2267205 and 12475124), a ZSTU intramural grant (22062267-Y) and Excellent Graduate Thesis Cultivation Fund (LW-YP2024011).

✉ Han-Kui Wang
whk2007@163.com

✉ You-Bao Wang
ybwang@ciae.ac.cn

[1] Key Laboratory of Physics, Zhejiang Sci-Tech University, Hangzhou 310018, China

[2] China Institute of Atomic Energy, Beijing 102413, China

missing physics and overfitting that existed in early semiempirical mass formulations, thereby reducing the root-mean-square error (*RMSD*) [28] to 1.92 MeV. Machine learning has important applications in nuclear physics because of its ability to handle complex problems, such as predicting half-life, charge radius and charge density [29–32]. By considering the α-decay energy and Garvey–Kelson relations (GKs) and applying the multiobjective optimization (MOO) method [13, 33, 34], Qian et al. significantly improved the theoretical accuracy of the BW2 model. Considering the isospin dependence, Bhagwat improved the liquid drop model to a model related to isospin and added fluctuation terms [35], which explained the binding energy of nucleons very well. Sequential least squares programming (SLSQP) [36] is a suitable algorithm for solving nonlinear optimization problems with constraints, because it can handle multiple constraints and nonlinear objective functions.

In this work, we studied an improved BW2 mass model with a higher-order term of symmetry energy [37] by employing certain algorithms, such as SLSQP. The mass models and algorithms are presented in Sect. 2. In Sect. 3, we test the generality of the SLSQP method using 200 sample mass formulae derived from randomly selected parameters of the E_{isospin} mass model. Finally, the conclusions are presented in Sect. 4.

2 Semiempirical Mass Formula

2.1 BW3 Mass model

The BW3 mass model is derived from the droplet model and improves the semiempirical mass formula [8–10] by incorporating additional physical constraints [37]:

$$\begin{aligned} B_{\mathrm{BW3}} =& \alpha_{\mathrm{V}}A + \alpha_{\mathrm{S}}A^{2/3} + \alpha_{\mathrm{C}}\frac{Z^2}{A^{1/3}} + \alpha_{\mathrm{t}}\frac{(N-Z)^2}{A} \\ &+ \alpha_{x\mathrm{C}}\frac{Z^{4/3}}{A^{1/3}} + \alpha_{\mathrm{W}}\frac{|N-Z|}{A} + \alpha_{\mathrm{st}}\frac{(Z-N)^2}{A^{4/3}} \\ &+ \alpha_{\mathrm{p}}\delta(N,Z)A^{-1/2} + \alpha_{\mathrm{R}}A^{1/3} + \alpha_{\mathrm{m}}P + \beta_{\mathrm{m}}P^2 \\ &+ \alpha_{\mathrm{pm}}\frac{(N-Z)^4}{A^3}. \end{aligned} \tag{1}$$

Equation (1) involves 12 parameters, and the $\delta(N,Z)$ is defined as

$$\delta(N,Z) = [(-1)^N + (-1)^Z]/2, \tag{2}$$

where 1 denotes even-even nuclei, -1 denotes odd-odd nuclei, and 0 denotes odd-A nuclei. P can be expressed as follows:

$$P = \frac{v_{\mathrm{p}}v_{\mathrm{n}}}{v_{\mathrm{p}} + v_{\mathrm{n}}}. \tag{3}$$

where v_{p} (v_{n}) represents the difference between $Z(N)$ and the nearby magic number.

$$\alpha_{\mathrm{pm}} = \frac{1}{162}\left(\frac{9\pi}{8}\right)^{\frac{2}{3}}\frac{\hbar^2}{mr_0^2}. \tag{4}$$

Equation (4) and its physical terms are derived from the application of the Fermi gas model to account for the nucleon binding energies. Following Pauli's exclusion principle, the nucleons (protons, neutrons and nuclei) are assumed to move freely within the nuclear volume. The potential experienced by each nucleon is a superposition of the potentials created by other nucleons. The Fermi gas model provides the total kinetic energy of the nucleons as follows:

$$\begin{aligned} \langle E(Z,N)\rangle =& N\langle E_N\rangle + Z\langle E_Z\rangle \\ =& \frac{3}{10m}\frac{\hbar^2}{r_0^2}\left(\frac{9\pi}{4}\right)^{\frac{2}{3}}\left(\frac{N^{\frac{5}{3}} + Z^{\frac{5}{3}}}{A^{\frac{2}{3}}}\right). \end{aligned} \tag{5}$$

Assuming that the radii of the proton and neutron potential wells are identical, a binomial expansion near $N = Z$ yields the following expression:

$$\begin{aligned} \langle E(Z,N)\rangle =& \frac{3}{10m}\frac{\hbar^2}{r_0^2}\left(\frac{9\pi}{8}\right)^{\frac{2}{3}}\left[A + \frac{5}{9}\frac{(N-Z)^2}{A}\right. \\ &\left. + \frac{5}{243}\frac{(N-Z)^4}{A^3} + \cdots\right]. \end{aligned} \tag{6}$$

The first term contributes to the volume in the mass formula, whereas the second corrects for $N \neq Z$. The third term represents a higher-order addition to the symmetry energy used to enhance the mass model.

2.2 E_{isospin} Mass model

The E_{isospin} mass formula can be expressed using Strutinsky's theorem [35]:

$$E_{\mathrm{isospin}}(Z,N) = -(E_{\mathrm{LDM}} + \delta E). \tag{7}$$

Here, E_{LDM} represents the macroscopic (M) section, which contains nine free parameters, hereafter referred to as M-parameters. The δE term corresponds to the fluctuation (F) of the binding energy and can generate more than 100 parameters, which are hereafter referred to as F-parameters. These F-parameters can be set as the parameter pool to form sample mass formulae to test the generality of these algorithms.

The macroscopic section includes the volume term related to the isotopic spin, the Coulomb term, the surface term, the Coulomb energy correction term related to surface diffusion and the pairing term.

$$\begin{aligned} E_{\mathrm{LDM}} =& \alpha_{\mathrm{V}}\left[1+\frac{4k_{\mathrm{V}}T_z(T_z+1)}{A^2}\right]A \\ &+\alpha_{\mathrm{S}}\left[1+\frac{4k_{\mathrm{S}}T_z(T_z+1)}{A^2}\right]A^{2/3} \\ &+\frac{3Z^2e^2}{5r_0A^{1/3}}+\frac{\alpha_{\mathrm{C}}Z^2}{A}+E_{\mathrm{p}}, \end{aligned} \tag{8}$$

where a_{V}, k_{V}, a_{S}, k_{S}, a_{C} and r_0 denote the volume energy, isospin dependence of the volume energy, surface energy, isospin dependence of the surface energy, Coulomb energy and Coulomb radius, respectively. T_Z is the third component of the isospin, and e is the electron charge.

For the correction, the smooth pairing energy [38] is given by

$$E_{\mathrm{p}}=\begin{cases} \frac{\lambda_{\mathrm{n}}}{N^{1/3}}, & Z \text{ even, } N \text{ odd,} \\ \frac{\lambda_{\mathrm{p}}}{N^{1/3}}, & Z \text{ odd, } N \text{ even,} \\ \frac{\lambda_{\mathrm{n}}}{N^{1/3}}+\frac{\lambda_{\mathrm{p}}}{N^{1/3}}+\frac{\lambda_{\mathrm{np}}}{N^{1/3}}, & Z,N \text{ odd,} \\ 0, & N,Z \text{ even.} \end{cases} \tag{9}$$

where λ_{n}, λ_{p} and λ_{np} are free parameters. The smooth pairing energy of even-even nuclei is zero because both protons and neutrons pair well in even-even nuclei.

δE can be expressed as

$$\delta E(\vec{x})=\sum_{\vec{k}=\vec{0}}^{\vec{M}}\left\{a_{\vec{k}}\cos\left(2\pi\frac{\vec{x}\cdot\vec{k}}{M}\right)+b_{\vec{k}}\sin\left(2\pi\frac{\vec{x}\cdot\vec{k}}{M}\right)\right\}, \tag{10}$$

where $\vec{k}\equiv(k_1,k_2,k_3,k_4)$ ($0\le k_i\le M$ for $i=1,2,3,4.$), and $\vec{x}\equiv(x_1,x_2,x_3,x_4)$:

$$\begin{aligned} &x_1=\beta_1\left|\frac{N-N_0}{N}\right|, \quad x_2=\beta_2\left|\frac{Z-Z_0}{Z}\right|, \\ &x_3=\beta_3N^{1/3}, \quad x_4=\beta_4Z^{1/3}. \end{aligned} \tag{11}$$

In this formula, $N_0(Z_0)$ is the nearby magic number, and β_1, β_2, β_3 and β_4 are the free parameters. The β_1 and β_2 describe the closeness to a shell closure given the proton and neutron conditions, respectively, and β_3 and β_4 are proportional to the Fermi momentum. The number of such parameters becomes quite large, $(2M^4+4)$, and not all the terms need to be expanded to M. Therefore, it can be simplified as

$$\begin{aligned} \delta E(\vec{x})=&\sum_{k_1=0}^{M}\sum_{k_2=0}^{M-k_1}\sum_{k_3=0}^{M-k_1-k_2}\sum_{k_4=0}^{M-k_1-k_2-k_3} \\ &\left\{a_{\vec{k}}\cos\left(2\pi\frac{\vec{x}\cdot\vec{k}}{M}\right)+b_{\vec{k}}\sin\left(2\pi\frac{\vec{x}\cdot\vec{k}}{M}\right)\right\}. \end{aligned} \tag{12}$$

This reduces the number of parameters to $\frac{1}{12}(M+4)!/M!+4$ because the mean of δE is approximately 0. Therefore, the free parameter can be further reduced to $\frac{1}{12}(M+4)!/M!+2$.

2.3 Algorithm principles

Several algorithms were investigated in this study: ordinary least squares (OLS) [39], SLSQP [36], Constrained Optimization by Linear Approximation (COBYLA) [40], Broyden–Fletcher–Goldfarb–Shanno (BFGS) [41] and conjugate gradient (CG) [42]. SLSQP, COBYLA and Trust-Constr [43] were found to be more effective algorithms for solving constrained optimization problems (COPs). To solve the COP in Eq. (9), SLSQP was used because it is the only algorithm that utilizes the information in the gradient and the Hessian matrix [44] to the fullest extent, resulting in faster convergence to the optimal solution.

$$\begin{aligned} &\min \quad f(\vec{x}) \\ &st \quad g(\vec{x})=0, h(\vec{x})\ge 0 \\ &\text{where} \quad \vec{x}=(x_1,x_2,x_3,\ldots,x_{k-2},x_{k-1},x_k)\in X \\ &\quad X=\vec{x}|\vec{l}\le\vec{x}\le\vec{u} \\ &\quad \vec{l}=(l_1,l_2,l_3,\ldots,l_{i-2},l_{i-1},l_i) \\ &\quad \vec{u}=(u_1,u_2,u_3,\ldots,u_{j-2},u_{j-1},u_j). \end{aligned} \tag{13}$$

In this formula, $\vec{x}$ is the solution vector, X is the vector space of solution vectors, $\vec{l}(\vec{u})$ is the upper (lower) bounds of the solution vector space, $g(\vec{x})$ is the equality constraint, $h(\vec{x})$ is the inequality constraint, and $f(\vec{x})$ is the objective optimization function [45].

The SLSQP algorithm iteratively minimizes the objective function under constraints using linear approximation. This transforms the constrained nonlinear problem into an unconstrained least squares problem. In each iteration, the gradient and Hessian matrix [44] were calculated to update the solution using Lagrange multipliers for the constraints.

$$L(\vec{x},\vec{\lambda},\vec{\mu})=f(\vec{x})+\vec{\lambda}^{\mathrm{T}}\times g(\vec{x})+\vec{\mu}^{\mathrm{T}}\times h(\vec{x}). \tag{14}$$

The superscript T denotes the transpose of the vector, and $\vec{\lambda}$ and $\vec{\mu}$ represent the penalty terms associated with the equality and inequality conditions, respectively [46].

An update rule is obtained for each iteration by solving an unconstrained least squares problem. This rule satisfies not only the equality and inequality constraints but also the first-order necessary conditions:

$$\nabla L(\vec{x},\vec{\lambda},\vec{\mu}) = \nabla f(\vec{x}) + J_g^{\mathrm{T}} \times \vec{\lambda} + J_h^{\mathrm{T}} \times \vec{\mu} = 0, \tag{15}$$

J_g and J_h are the Jacobian matrices of the equality and inequality constraints, respectively [47].

According to the above update rule, the initial value $\vec{x}_1$ is chosen, and the stopping criterion ε is set. The gradient vector $\nabla f_k(\vec{x}_k)$ is computed at each iteration, k. If $||\nabla f_k(\vec{x}_k)|| < \varepsilon$, the algorithm is terminated and an approximate solution $\vec{x}^*$ is obtained. This process constructs a sequential programming model as follows:

$$\begin{aligned} \min \quad & q(\vec{x}) = f_k(\vec{x}) + g_k^T(\vec{x}-\vec{x}_k) \\ & \quad + \frac{1}{2}(\vec{x}-\vec{x}_k)^T B_k(\vec{x}-\vec{x}_k) \\ st \quad & A_{\mathrm{eq}}(\vec{x}-\vec{x}_0) = 0 \\ & g_k(\vec{x}) \geq 0, k = 1,2,\ldots,k. \end{aligned} \tag{16}$$

In this formula, B_k is a positive definite symmetric matrix used to approximate the inverse of the Hessian matrix and A_{eq} is the Jacobian matrix of the equality constraints.

This model is solved to obtain the modified direction $\Delta\vec{x}$ by computing the step size α such that the objective function decreases sufficiently along the search direction:

$$\begin{aligned} \alpha &= \min(1, r) \\ r &= \max(\beta_{\mathrm{s}}, r_{\mathrm{t}}) \\ \beta_{\mathrm{s}} &= \left(\frac{\partial f}{\partial \vec{x}}\right)^{\mathrm{T}} (\Delta\vec{x}/s) \\ r_{\mathrm{t}} &= \left(\frac{\partial g}{\partial \vec{x}}\right)^{\mathrm{T}} (\Delta\vec{x}/t), \end{aligned} \tag{17}$$

where s and t are positive scale factors. Finally, the estimated points are updated as follows: $\vec{x}_{k+1} = \vec{x}_k + \alpha\Delta\vec{x}$. By solving the system of equations above following this iterative process, the objective function is gradually enhanced to determine the optimal solution that satisfies the constraints.

3 Discussion

The coefficients of the BW3 model are improved with less error between the calculated values and experimental data using the SLSQP algorithm [36]. Subsequently, the following constraints were incorporated to guarantee the physical viability of the program calculations:

1. The nuclide numbers should satisfy $N \geq 8$ and $Z \geq 8$.
2. After satisfying Condition 1, the specific binding energy of the remaining nuclides, $\frac{B_{\mathrm{Th}}}{N+Z}$, is distributed in the range of $5-9$ MeV.

The performance metrics of the model were evaluated using *RMSD* [28], which is defined as follows:

$$RMSD = \sqrt{\frac{\sum_{i=1}^{n}(B_{\mathrm{Ex}_i} - B_{\mathrm{Th}_i})^2}{n}}, \tag{18}$$

where n represents the total number of nuclides involved in the calculation and B_{Ex_i} and B_{Th_i} are the current experimental and theoretical nuclide binding energies, respectively.

The modified coefficients corresponding to several algorithms are listed in Table 1. Different algorithms can lead to alterations in the weights of the terms within the model, as listed in table. The weights signify the degree to which each term affects the model and the symbols denote positive or negative corrections. The volume, surface, symmetry, Wigner, surface symmetry, pairing, higher-order correction and curvature terms have high weights because of their significant influence on the mass model, whereas the Coulomb, Coulomb exchange, and shell effect terms [21–27] have low weights because of their relatively minor influence. In the plot, the horizontal coordinate represents the number of neutrons N, and the vertical coordinate

Table 1 Coefficients of the BW3 mass model under each algorithm for binding energy (in MeV)

	OLS	SLSQP	BFGS	Trust-Constr	L-BFGS-B	CG
α_{V}	16.58	16.05	16.05	16.03	15.19	16.20
α_{S}	−26.95	−23.10	−23.10	−22.96	−16.47	−23.33
α_{C}	−0.774	−0.74	−0.74	−0.74	−0.71	−0.74
α_t	−31.51	−31.62	−31.62	−31.53	−25.83	−31.50
α_{xC}	2.22	1.59	1.59	1.59	1.42	1.39
α_{W}	−43.40	−72.96	−72.97	−72.14	5.39	−57.06
α_{st}	55.62	64.10	64.10	63.59	23.84	54.80
α_{p}	9.87	10.56	10.56	10.56	12.36	10.63
α_{R}	14.77	9.89	9.89	9.64	−4.19	9.87
α_{m}	−1.90	−1.88	−1.88	−1.88	−1.82	−1.89
β_{m}	0.14	0.14	0.14	0.14	0.14	0.14
α_{pm}	−1.30	−11.36	−11.36	−11.31	−1.13	0.14

represents the percentage of the relative error [12], which is defined as

$$\frac{\delta B}{B}(\%) = \frac{B_{\mathrm{Ex}} - B_{\mathrm{Th}}}{B_{\mathrm{Ex}}} \times 100\%. \tag{19}$$

The errors exhibit different trends for different nuclide regions under different algorithms. Figure 1a, 1b and 1c shows a reduction in the overall error and a narrowing of the fluctuation range of the light and medium nuclide regions. In Fig. 1e and 1f, the fluctuation amplitude of the heavy nuclide regions increases, which leads to an increase in the fluctuation amplitude of the light nuclide regions, such that the total *RMSD* does not decrease or even deteriorate. SLSQP [36] exhibits greater

advantages in reducing model errors when comparing performance metrics, such as $\frac{\delta B}{B}(\%)$ [12] and *RMSD* [28] of the mass model obtained using different algorithms. This is attributed to the reduced weights of the surface and curvature terms by SLSQP and the increased weights of Wigner, surface symmetry, pairing and higher-order correction terms. The results also show that in Atomic Mass Evaluation (AME2020), the influence of the surface and curvature terms on the binding energy decreases, whereas that of the Wigner, surface symmetry, pairing and higher-order correction terms on the overall effect increases. This also indicates that the mass model under SLSQP not only reduces the impact of the surface and curvature terms on the binding energy but also enhances the impact of the Wigner term on the overall effect, thereby improving its extrapolation ability [17, 18] and more accurately reflecting the contributions of different physical terms to the binding energy.

Figure 2 shows the relative error between the theoretical and experimental values of the BW3 mass model obtained by employing the SLSQP and OLS algorithms, where the *x*-axis represents the neutron number, the *y*-axis represents the atomic number, and the *z*-axis corresponds to the relative error percentage $\frac{\delta B}{B}(\%)$. In the figure, the fluctuations in the differences are more pronounced for the magic nuclei, particularly those nuclei in the vicinity of the doubly magic nuclei, which imply distinct interactions between the magic and nonmagic nuclei. The SLSQP improves the error near the doubly magic nuclei, captures the special interaction effects around the magic nuclei more accurately and thus enhances the accuracy of the theoretical model.

Figure 3 shows the performance of the SLSQP algorithm with regard to even-even, odd-odd and odd-*A* nuclei. The optimization effect of the SLSQP algorithm on different types of nuclei exhibits significant differences. The improvement is most pronounced for even-even nuclei, whereas certain optimization results can also be attained for odd-*A* and odd-odd nuclei. Figure 3a shows that for even-even nuclei [48] (both *Z* and *N* are even), the SLSQP algorithm provides a significant reduction in *RMSD* [28] by 0.29 MeV, with a performance improvement of approximately 15.18%, achieving a more substantial optimization in the entire nuclei region compared with the theoretical value of the BW3 model with OLS coefficients. In Fig. 3b, for odd-*Z* and even-*N* nuclei, after the SLSQP optimization, the model *RMSD* is reduced by 0.19 MeV, with a performance improvement of approximately 9.79%. Similarly, in Fig. 3c,

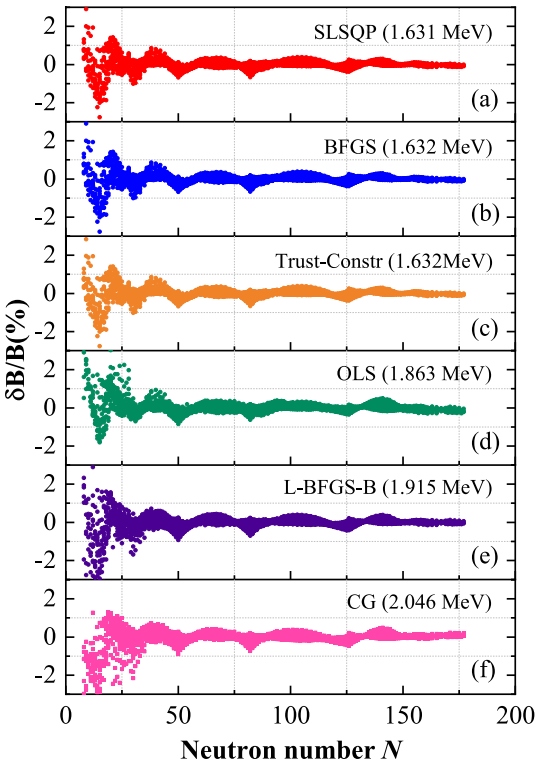

Fig. 1 (Color online) BW3 mass model relative error comparison using different algorithms, and its *RMSD* is shown in parentheses

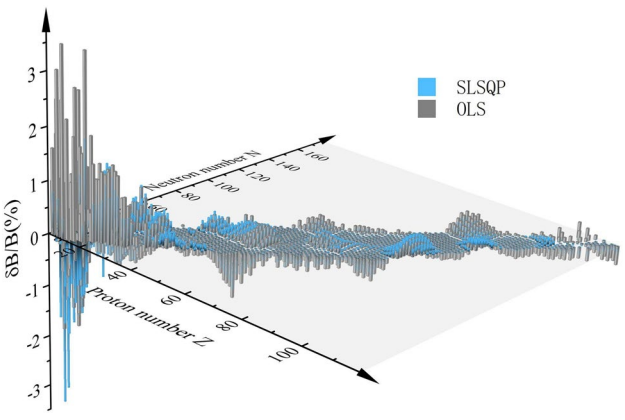

Fig. 2 (Color online) BW3 mass model relative error comparison with SLSQP/OLS coefficients

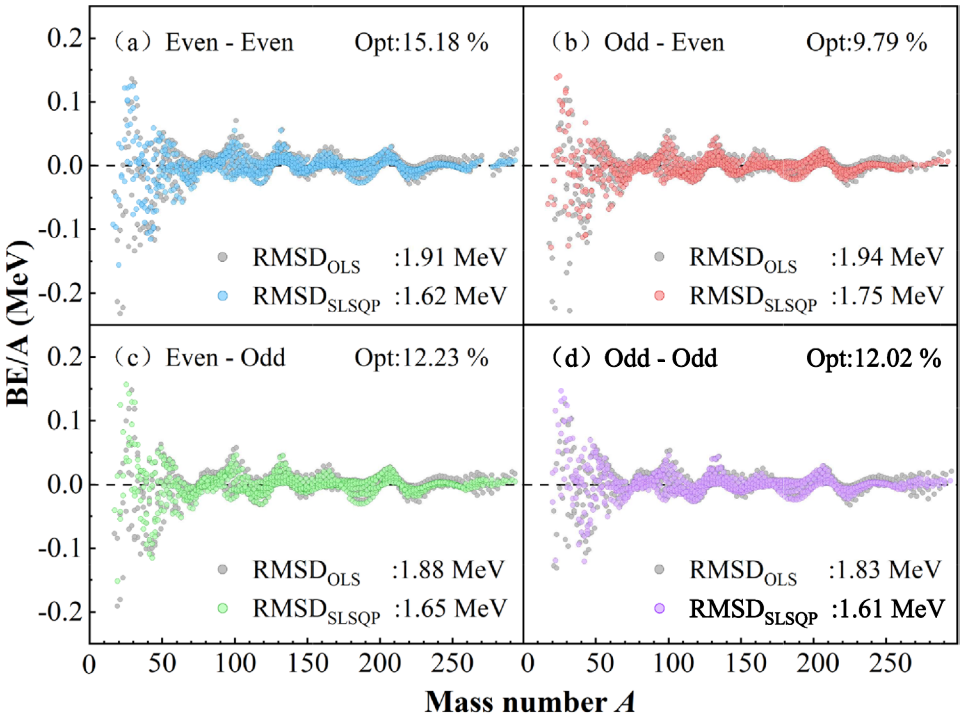

Fig. 3 (Color online) BW3 mass model performance on total nuclei with SLSQP/OLS coefficients

for even-Z and odd-N nuclei, the model $RMSD$ is reduced by 0.23 MeV, with a performance improvement of approximately 12.23%. Notably, in the medium-nuclei region, the optimization results are closer to the experimental values. For odd-odd nuclei (both Z and N are odd), Fig. 3d shows that after SLSQP optimization, the model $RMSD$ is reduced by 0.22 MeV and the performance is improved by approximately 12.02%. In particular, in the heavy-nuclei region, the optimization results are closer to the experimental values. These results further validate the effectiveness of the SLSQP algorithm for mass model optimization.

To test the generality of the SLSQP method, we devised 200 sample mass formulae by randomly selecting parameters from the F-parameters in the δE term of the E_{isospin} mass model. As mentioned previously, the E_{isospin} mass model consists of two parts: the E_{LDM} term, which contains nine M-parameters derived from the liquid drop model, and the δE term, which encompasses more than 100 F-parameters. If we set $M = 4$ in the E_{isospin} mass model, then 144 F-parameters are obtained. Subsequently, we compared the results with the nuclear mass dataset AME2020 and found that the $RMSD$ was 1.268 MeV in this situation. Next, we tested the contributions of these F-parameters individually and identified 53 parameters that had obvious effects on the binding energy. Subsequently, we randomly selected 10 F-parameters from the 53 F-parameters and combined them with nine M-parameters to form a sample mass formula. Thus, we devised 200 sample mass formulas to test the proposed algorithms presented in this work. The SLSQP method outperformed the other algorithms in terms of both error and convergence speed.

As shown in Fig. 4, the SLSQP algorithm performs significantly better than the BFGS and L-BFGS-B algorithms. For example, at the 48th sample point, the $\triangle RMSD$ of the SLSQP algorithm was 4 MeV, whereas those of BFGS and L-BFGS-B were 23.9 MeV and 23.0 MeV, respectively. At the 67th sample point, the $\triangle RMSD$ of the SLSQP algorithm was 2.7 MeV, whereas those of BFGS and L-BFGS-B

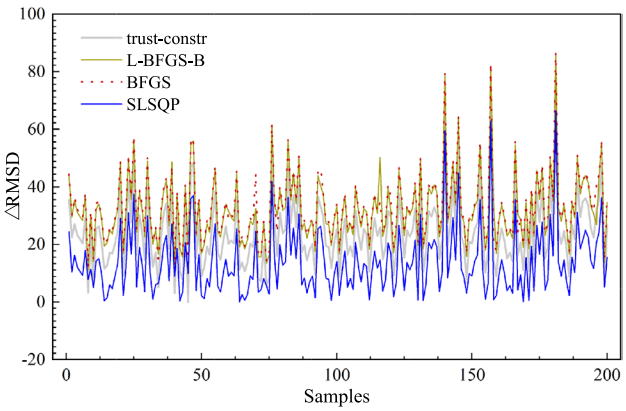

Fig. 4 (Color online) Finding 62 important parameters from the δE term of the E_{isospin} mass model, randomly selecting 10 items as a sample formula with E_{LDM}, and obtaining 200 samples of mass formulas. The $\triangle RMSD$ is defined as $(RMSD - RMSD_{\text{min}}) \times 100$, where $RMSD_{\text{min}}$ is the minimum root-mean-square deviation optimized by the algorithm for 200 samples

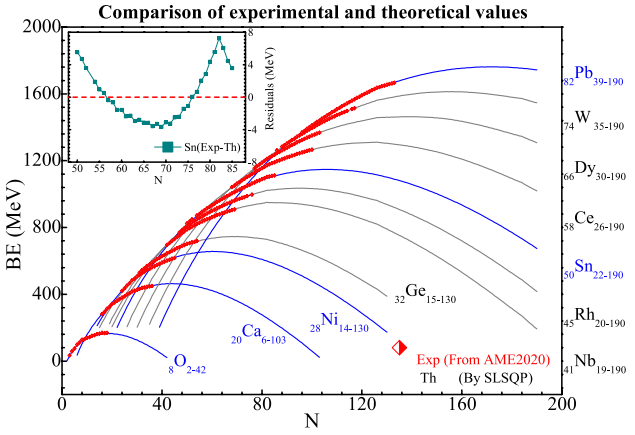

Fig. 5 (Color online) Experimental binding energy values from the AME2020 [6, 7], and the theoretical predicted value by the SLSQP method

were 22.7 MeV and 21.8 MeV, respectively. However, the Trust-Constr algorithm exhibits a large error amplitude, which results in poor stability during parameter optimization. In terms of computational efficiency, compared with the SLSQP algorithm as a reference, the BFGS takes approximately 2.44 times longer, L-BFGS-B takes around 2.78 times longer, and the Trust-Constr takes a staggering 8.44 times longer. The SLSQP algorithm not only has good stability with small root-mean-square errors, but also high computational efficiency.

To verify the effectiveness of the SLSQP algorithm, the experimental and theoretical values were compared, as illustrated in Fig. 5. The experimental binding energy values were obtained from AME2020, whereas the theoretical values were obtained by optimizing the BW3 mass model using the SLSQP method. Among the experimental values, the maximum binding energy for the O isotopes is currently measured at $^{24}O_{16}$, with a binding energy value of 168.95 MeV. Beyond this isotope, the binding energy decreases as N increases. The SLSQP-optimized theoretical model predicts the maximum point to be at $^{26}O_{18}$ with a binding energy value of 168.95 MeV, followed by a similar decline in the binding energy with an increase in N. For the other isotope chains, the experimental binding energy values exhibit an overall increasing trend without reaching a maximum. By optimizing the BW3 nuclear mass model using the SLSQP method, the following maximum binding energy points are predicted for these isotope chains: ^{64}Ca = 464.33 MeV , ^{88}Ni = 656.72 MeV , ^{123}Nb = 950.29 MeV , ^{141}Rh = 1035.66 MeV, ^{100}Ge = 745.77 MeV, ^{156}Sn = 1148.31 MeV, ^{184}Ce = 1311.84 MeV, ^{206}Dy = 1463.63 MeV, ^{230}W = 1613.36 MeV, ^{252}Pb = 1761.89 MeV.

4 Conclusion

In this study, we investigated an improved mass model with a higher-order symmetry energy term by employing several algorithms. The SLSQP algorithm demonstrated the best performance in terms of both root-mean-square errors and computational efficiency. This algorithm reduced the global *RMSD* from 1.863 MeV to 1.631 MeV (12.45% reduction). The odd (even) numbers of protons and neutrons are discussed, and the SLSQP algorithm reduced the local *RMSD* from 1.91 MeV to 1.62 MeV (15.18% optimization) when the nuclei have even numbers of both protons and neutrons. The local *RMSD* is reduced from 1.83 MeV to 1.61 MeV when the nuclei have odd numbers of protons and neutrons. With an odd (even) number of protons (neutrons), the local *RMSD* decreases from 1.94 MeV to 1.75 MeV (9.79% optimization). The local *RMSD* is reduced from 1.88 MeV to 1.65 MeV (12.23% optimization) when the number of protons is even and the number of neutron is odd. We tested these algorithms using 200 sample mass formulas derived from the E_{isospin} mass model. Each sample mass formula includes 19 free parameters, of which nine are M-parameters derived from the liquid drop model and 10 are F-parameters from the δE term of the E_{isospin} mass model. The SLSQP method provides better performance than the other algorithms in terms of errors and convergence speed. According to this study, the SLSQP algorithm is suitable for handling large-scale multiparameter optimization tasks in nuclear physics.

Author contributions All authors contributed to the study conception and design. Material preparation, data collection and analysis were performed by Hang Yang, Cun-Yu Chen, Xiao-Yu Xu, Han-Kui Wang and You-Bao Wang. The first draft of the manuscript was written by Hang Yang, and all authors commented on previous versions of the manuscript. All authors read and approved the final manuscript.

Data availability The data that support the findings of this study are openly available in Science Data Bank at https://cstr.cn/31253.11.sciencedb.j00186.00656 and https://doi.org/10.57760/sciencedb.j00186.00656.

Declarations

Conflict of interest The authors declare that they have no competing interests.

References

1. B. Michael, P.H. Heenen, P.G. Reinhard, Self-consistent mean-field models for nuclear structure. Rev. Mod. Phys **75**, 121–180 (2003). https://doi.org/10.1103/RevModPhys.75.121
2. D. Lunney, J.M. Pearson, C. Thibault, Recent trends in the determination of nuclear masses. Rev. Mod. Phys **75**, 1021–1082 (2003). https://doi.org/10.1103/RevModPhys.75.1021

3. A.C. Larsen, A. Spyrou, S.N. Liddick et al., Novel techniques for constraining neutron-capture rates relevant for r-process heavy-element nucleosynthesis. Prog. Part. Nucl. Phys **107**, 69–108 (2019). https://doi.org/10.1016/j.ppnp.2019.04.002
4. T. Yamaguchi, H. Koura, M. Wang et al., Masses of exotic nuclei. Prog. Part. Nucl. Phys **120**, 103882 (2021). https://doi.org/10.1016/j.ppnp.2021.103882
5. J. Erler, N. Birge, M. Kortelainen et al., The limits of the nuclear landscape. Nature **486**, 509–512 (2012). https://doi.org/10.1038/nature11188
6. W.J. Huang, M. Wang, F.G. Kobdev et al., The AME 2020 atomic mass evaluation (I). Evaluation of input data, and adjustment procedures. Chinese Phys. C **45**, 030002 (2021). https://doi.org/10.1088/1674-1137/abddb0
7. M. Wang, W.J. Huang, F.G. Kobdev et al., The AME 2020 atomic mass evaluation (II). Tables, graphs and references. Chinese Phys. C **45**, 030003 (2021). https://doi.org/10.1088/1674-1137/abddaf
8. P. Möller, A.J. Sierk, T. Ichikawa et al., Nuclear ground-state masses and deformations: FRDM(2012). At. Data Nucl. Data Tables **109–110**, 1–204 (2016). https://doi.org/10.1016/j.adt.2015.10.002
9. C.F. v. Weizsäcker, Zur Theorie der Kernmassen. Z. Physik **96**, 431–458 (1935). https://doi.org/10.1007/BF01337700
10. H.A. Bethe, R.F. Bacher, Nuclear physics A. Stationary states of nuclei. Rev. Mod. Phys **8**, 82 (1936). https://doi.org/10.1103/RevModPhys.8.82
11. B. Mohammed-Azizi, Better insight into the Strutinsky method. Phys. Rev. C **100**, 034319 (2019). https://doi.org/10.1103/PhysRevC.100.034319
12. D. Benzaid, S. Bentridi, A. Kerraci et al., Bethe-Weizsacker semiempirical mass formula coefficients 2019 update based on AME2016. Nucl. Sci. Tech **31**, 9 (2020). https://doi.org/10.1007/s41365-019-0718-8
13. W.H. Ye, Y.B. Qian, Z.Z. Ren, Accuracy versus predictive power in nuclear mass tabulations. Phys. Rev. C **106**, 024318 (2022). https://doi.org/10.1103/PhysRevC.106.024318
14. P. Möller, W.D. Myers, H. Sagawa et al., New finite-range droplet mass model and equation-of-state parameters. Phys. Rev. Lett **108**, 052501 (2012). https://doi.org/10.1103/PhysRevLett.108.052501
15. H. Koura, T. Tachibana, M. Uno et al., Nuclidic mass formula on a spherical basis with an improved even-ddd term. Prog. Theor. Phys **113**, 305 (2005). https://doi.org/10.1143/PTP.113.305
16. F.A. Ivanyuk, K. Pomorski, Optimal shapes and fission barriers of nuclei within the liquid drop model. Phys. Rev. C **79**, 054327 (2009). https://doi.org/10.1103/PhysRevC.79.054327
17. S. Goriely, N. Chamel, J.M. Pearson, Further explorations of Skyrme-Hartree-Fock-Bogoliubov mass formulas. XII. Stiffness and stability of neutron-star matter. Phys. Rev. C **82**, 035804 (2010). https://doi.org/10.1103/PhysRevC.82.035804
18. S. Goriely, N. Chamel, Further explorations of Skyrme-Hartree-Fock-Bogoliubov mass formulas. XIII. The 2012 atomic mass evaluation and the symmetry coefficient. Phys. Rev. C **88**, 024308 (2013). https://doi.org/10.1103/PhysRevC.88.024308
19. R.A. Rego, Mean free path in the relativistic mean field. Phys. Rev. C **44**, 1944 (1991). https://doi.org/10.1103/PhysRevC.44.1944
20. J.L. Janssen, Y. Gillet, A. Martin et al., Precise effective masses from density functional perturbation theory. Phys. Rev. B **93**, 205147 (2016). https://doi.org/10.1103/PhysRevB.93.205147
21. W.K. Michael, Mutual influence of terms in a semi-empirical mass formula. Nucl. Phys. A. **798**, 29–60 (2008). https://doi.org/10.1016/j.nuclphysa.2007.10.011
22. D.M. William, J.S. Wladyslaw, Nuclear masses and deformations. Nucl. Phys **81**, 1–60 (1966). https://doi.org/10.1016/S0029-5582(66)80001-9
23. A.N. Antonov, D.N. Kadrev, M.K. Gaidarov et al., Temperature dependence of the symmetry energy and neutron skins in Ni, Sn, and Pb isotopic chains. Phys. Rev. C **95**, 024314 (2017). https://doi.org/10.1103/PhysRevC.95.024314
24. T. Naito, R. Akashi, H.Z. Liang, Application of a Coulomb energy density functional for atomic nuclei: Case studies of local density approximation and generalized gradient approximation. Phys. Rev. C **97**, 044319 (2018). https://doi.org/10.1103/PhysRevC.97.044319
25. G. Lugones, A.G. Grunfeld, Surface and curvature properties of charged strangelets in compact objects. Phys. Rev. C **103**, 035813 (2021). https://doi.org/10.1103/PhysRevC.103.035813
26. E. Wigner, On the consequences of the symmetry of the nuclear Hamiltonian on the spectroscopy of nuclei. Phys. Rev **51**, 106 (1937). https://doi.org/10.1103/PhysRev.51.106
27. R.F. Casten, Nuclear structure from a simple perspective. Oxford. Acad. **32**, 358–358 (2001). https://doi.org/10.1093/acprof:oso/9780198507246.001.0001
28. G. Royer, C. Gautier, Coefficients and terms of the liquid drop model and mass formula. Phys. Rev. C **73**, 067302 (2006). https://doi.org/10.1103/PhysRevC.73.067302
29. Z.M. Niu, H.Z. Liang, Nuclear mass predictions based on Bayesian neural network approach with pairing and shell effects. Phys. Lett. B **778**, 48–53 (2018). https://doi.org/10.1016/j.physletb.2018.01.002
30. B.S. Cai, C.X. Yuan, Random forest-based prediction of decay modes and half-lives of superheavy nuclei. Nucl. Sci. Tech **34**, 204 (2023). https://doi.org/10.1007/s41365-023-01354-5
31. Y.Y. Cao, J.Y. Guo, B. Zhou, Predictions of nuclear charge radii based on the convolutional neural network. Nucl. Sci. Tech **34**, 152 (2023). https://doi.org/10.1007/s41365-023-01308-x
32. T.S. Shang, J. Li, Z.M. Niu, Prediction of nuclear charge density distribution with feedback neural network. Nucl. Sci. Tech **33**, 153 (2022). https://doi.org/10.1007/s41365-022-01140-9
33. W.H. Ye, Y.B. Qian, H.K. Wang, Multiple constraints on nuclear mass formulas for reliable extrapolations. Phys. Rev. C **107**, 044302 (2023). https://doi.org/10.1103/PhysRevC.107.044302
34. G.T. Garvey, W.J. Gerace, R.L. Jaffe et al., Set of nuclear-mass relations and a resultant mass table. Rev. Mod. Phys **41**, S1–S80 (1969). https://doi.org/10.1103/RevModPhys.41.S1
35. A. Bhagwat, Simple nuclear mass formula. Phys. Rev. C **90**, 064306 (2014). https://doi.org/10.1103/PhysRevC.90.064306
36. M. Gong, F. Zhao, S.Y. Zeng et al., An experimental study on local and global optima of linear antenna array synthesis by using the sequential least squares programming. Appl. Soft. Comput. **148**, 110859 (2023). https://doi.org/10.1016/j.asoc.2023.110859
37. X.Y. Xu, L. Deng, A.X. Chen et al., Improved nuclear mass formula with an additional term from the Fermi gas model. Nucl. Sci. Tech **35**, 91 (2024). https://doi.org/10.1007/s41365-024-01450-0
38. P. Möller, J.R. Nix, Nuclear pairing models. Nucl. Phys. A **536**, 20–60 (1992). https://doi.org/10.1016/0375-9474(92)90244-E
39. K. Lakshmi, B. Mahaboob, M. Rajaiah et al., Ordinary least squares estimation of parameters of linear model. J. Math. Comput. Sci. **11**, 2015–2030 (2021). https://doi.org/10.28919/jmcs/5454
40. B. Rao, L. Yang, S.H. Zhong et al., Robust approximation of chance constrained optimization with polynomial perturbation. Comput. Optim. Appl. **89**, 977–1003 (2024). https://doi.org/10.1007/s10589-024-00602-7
41. F. Flachsenberg, M. Rarey, LSLOpt: An open-source implementation of the step-length controlled LSL-BFGS algorithm. J. Comput. Chem. **42**, 1095–1100 (2021). https://doi.org/10.1002/jcc.26522
42. Y.L. Lu, W.Y. Li, C.M. Zhang et al., A class new hybrid conjugate gradient method for unconstrained optimization. J. Comput.

Chem. **12**, 1941–1949 (2015). https://api.semanticscholar.org/CorpusID:124611131
43. Y.G. Pei, D.T. Zhu, On the global convergence of a projective trust region algorithm for nonlinear equality constrained optimization. Acta. Math. Sin.-English Ser. **34**, 1804–1828 (2018). https://doi.org/10.1007/s10114-018-7063-4
44. P.G. Chen, Y.J. Peng, S.J. Wang, The Hessian matrix of Lagrange function. Linear. Algebra. Appl. **531**, 537–546 (2017). https://doi.org/10.1016/j.laa.2017.06.012
45. F.S.P.S. Abad, M. Allahdadi, H.M. Nehi, Interval linear fractional programming: optimal value range of the objective function. Comp. Appl. Math **39**, 261 (2020). https://doi.org/10.1007/s40314-020-01308-2
46. D.M. Hou, Y.X. Ning, C. Zhang, An efficient and robust Lagrange multiplier approach with a penalty term for phase-field models. J. Comput. Phys **488**, 112236 (2023). https://doi.org/10.1016/j.jcp.2023.112236
47. P. Armand, N.N. Tran, Boundedness of the inverse of a regularized Jacobian matrix in constrained optimization and applications. Optim. Lett **16**, 2359–2371 (2022). https://doi.org/10.1007/s11590-021-01829-7
48. Z.M. Niu, B.H. Sun, H.Z. Liang et al., Improved radial basis function approach with odd-even corrections. Phys. Rev. C **94**, 054315 (2016). https://doi.org/10.1103/PhysRevC.94.054315